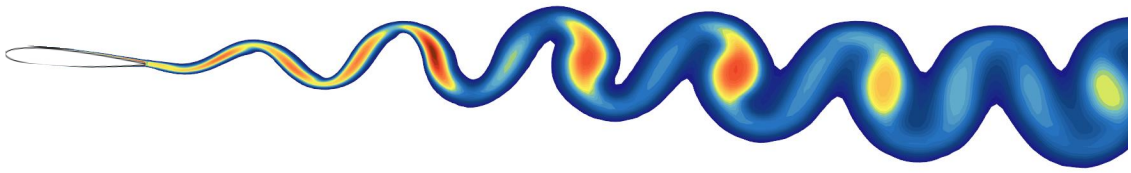

Fluid-Structure Interaction; Stiffness Effects on Airfoil Flutter

A numerical study of airfoil flutter in STAR-CCM+

Extensive Project Report, Engineering Fluid-Structure Interaction: Technologies and Practices

OSKAR TYLÉN

Master Program Applied Mechanics
CHALMERS UNIVERSITY OF TECHNOLOGY
Gothenburg, Sweden 2022
www.chalmers.se

Extensive Project Report

Fluid-Structure Interaction; Stiffness Effects on Airfoil Flutter

A numerical study of airfoil flutter in STAR-CCM+

OSKAR TYLÉN

CHALMERS
UNIVERSITY OF TECHNOLOGY

Master Program Applied Mechanics
Chalmers University of Technology
Gothenburg, Sweden 2022

Fluid-Structure Interaction; Stiffness Effects on Airfoil Flutter
A numerical study of airfoil flutter in STAR-CCM+
OSKAR TYLÉN
Master Program Applied Mechanics
Chalmers University of Technology

Abstract

This report looks in to the phenomenon called *flutter*, a type of flow induced vibration in structures occurring at specific flow conditions. Specifically, the project looks at how flutter affects airfoils, and how the structural stiffness of the airfoil impacts the flutter effects at a certain set of conditions.
The analysis was carried out using commercial CFD solver *STAR-CCM+*. Within this software, the structural dynamics of a symmetric NACA0012 airfoil were modeled as a two-degree-of-freedom system with one bending mode and one torsional mode. Due to constraints on computational power and time, the mesh generation was adjusted to reduce computational time as much as possible without it effecting the behaviour of certain parameters, particularly the aerodynamic lift coefficient which was considered an important performance measure for the airfoil.
The results indicate that with a given set of operating conditions, adjusting the structural stiffness can be used as an effective countermeasure against flutter. However due to the mesh limitations mentioned above, the quality of the results can be questioned when looking closer at the flow field and numerical instabilities effecting some parameters.

Keywords: Fluid Structure Interaction, FSI, Flow Induced Vibrations, Airfoil Flutter, STAR-CCM+, Structural Dynamics

List of Acronyms

Below is the list of acronyms that have been used throughout this report listed in alphabetical order:

CAE	Computer Aided Engineering
CFD	Computational Fluid Dynamics
FEM	Finite Element Method

Nomenclature

Below is the nomenclature of indices and variables that have been used throughout this report.

Indices

∞	Indicates free stream parameter
0	indicates initial value

Variables

k_{fac}	Variable used to increase/decrease structural stiffness in increments
c	Airfoil chord length
t	Maximum airfoil thickness
L	Aerodynamic lift force
ρ	Fluid density
v	Fluid Velocity
v_r	Reduced Velocity
D	Characteristic length for reduced velocity
S_{ref}	Lift coefficient reference surface
C_{L}	Aerodynamic lift coefficient
α	Airfoil incidence
$\mathbf{M}$	Modal mass matrix
$\mathbf{u}$	Degree-of-freedom vector
$\mathbf{K}$	Modal stiffness matrix
M	Airfoil mass
y	y-coordinate of elastic axis
k_y	Bending stiffness
I_α	Moment of inertia around elastic axis
k_α	Torsional stiffness

x_α	Distance between airfoil center of gravity and elastic axis

Contents

List of Figures

List of Tables

1

Introduction

An important aspect when designing aircraft wings, turbine blades and similar components is the structural vibrations that can be induced by the flow field at certain conditions. One such condition is when the flow reaches a velocity where the structure cannot fully dissipate the energy extracted from the flow. This energy is then transferred to the structure in form of vibrations. This phenomenon is called **flutter**, and is examined in this project.

1.1 Task Description

The task preceding this report was to simulate the flutter of an airfoil subjected to certain flow conditions. In order to simplify the problem, the structural motion of the airfoil was reduced to two degrees of freedom constrained by torsional and flexural springs. This allowed for the analysis of the behavior of a system with two eigenmodes, and alleviated the need for coupling of CFD and FEM solvers.

The initial conditions to be used in the simulations were given, and can be found in table 1.1

Airfoil	
Geometry	NACA0012
Chord length	1 m
Material	Aluminium
Position of elastic axis	40 % of chord length
Flexural stiffness	508280 N/m % of chord length
Torsional stiffness	6269.75 Nm/rad
Fluid	
Type	Compressible dry air at 21°C
Velocity	50 m/s
Pressure	101325 Pa

Table 1.1: Given conditions for the simulation case

The main goal of the report is to examine how changes to the airfoil stiffness changes its proneness to flutter, and to examine the quality of the simulation settings and meshes used within the limitations of the project.

1.2 Limitations

Given the total length of the project, as well as the computational power available, it is not possible to run simulations at the fidelity required to get results independent of mesh. To make sure that the simulations would not have to run for multiple days, the mesh and solver settings were designed and chosen so that the simulation for one case could run over night. On the 4 CPU-core desktops available, and 5 seconds of physical time required to catch the existence of flutter effects, this resulted in the mesh described in section 4.1 and the resulting numerical issues described in section 4.2.3.

2

Theory

From years of development within the aerospace- and energy sectors, there is plenty of theory on fluid flow around airfoils. Naturally this ranges from modern CAE implementations to simplified theoretical methodology backed by experimental results. The theory surrounding structural dynamics of airfoils may not be quite as progressed, however there are simplified models that can be used to describe the torsional- and bending dynamics of airfoils. In addition to this, modern FEM driven structural dynamics is a powerful tool that can be used to analyze the airfoil vibration.

In this chapter, we have look at the at the methods suitable for the purpose and limitations of this project.

2.1 NACA Airfoils

During the 1920s and 1930s, the National Advisory Committee for Aeronautics developed airfoils that could be described using a 4-digit number, e.g. NACAXXXX. The initial two digits describe airfoil camber and the remaining two describe maximum airfoil thickness. Symmetrical airfoils with no camber can hence be described as NACA00XX. The symmetry make these airfoils particularly useful for somewhat simpler aerodynamic analysis than airfoils of more complex shape.

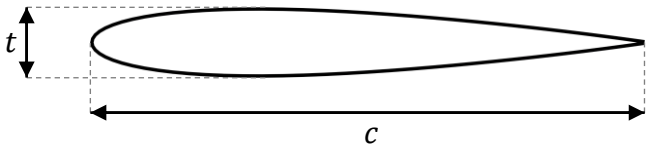

Figure 2.1: Sketch of an arbitrary symmetrical NACA airfoil. The chord length is denoted c and the maximum thickness is denoted t

For this project, the NACA0012 airfoil with a 1 meter chord length was used. With the nomenclature of figure 2.1 we have $t = 0.12$ cm and $c = 1$ m.

Thin airfoil theory

The lift force acting on an object is often calulated as

$$L = \frac{1}{2}\rho V_\infty S_{ref} C_\mathrm{L}$$

Where C_L is the non-dimensional lift coefficient. Among the most basic theories of how to determine this coefficient for airfoils one finds *thin airfoil theory*. The lift coefficient is assumed to vary linearly with the airfoil angle of attack α.[1]

$$C_{\mathrm{L}} = 2\pi\alpha \tag{2.1}$$

This theory rests on a number of assumptions, making it rather useless for accurate analysis of complex flows. However it can be useful for basic analysis and understanding of the forces acting on an airfoil at small angles of attack.

2.2 Flutter Theory and Structural Dynamics

An elastically supported body subjected to static flow conditions will normally only vibrate slightly in its degrees-of-freedom. However at certain conditions, the vibratory motion induces "*negative damping*" leading to dynamic instability.[2] One example of this phenomena is *bending - torsion* flutter, which results from the coupling between bending and torsional modes. For a specific system, instability appears when the flow velocity exceeds a critical value as the phase and amplitude combination of the structural modes extract energy from the flow.[3]

2.2.1 Structural Modes and Eigenvalues

The structural dynamics of an undamped system in free vibration are governed by the structural dynamics equation

$$\boldsymbol{M}\ddot{\boldsymbol{u}}(t) + \boldsymbol{K}\boldsymbol{u}(t) = \boldsymbol{0} \tag{2.2}$$

Assuming that the displacement is governed by time function $\boldsymbol{u}(t) = \hat{\boldsymbol{u}}e^{i\omega t}$ leads to the characteristic equation

$$\boldsymbol{K} - \omega^2\boldsymbol{M} = \boldsymbol{0}$$

Solving the characteristic equation gives the eigenvalues ω^2, which in turn lead to the systems natural frequencies ω, one for each degree of freedom. [4]

For an undamped two-degree-of-freedom rigid airfoil in free vibration the motion can be described by the coupled differential equations[5]

$$M\ddot{y} - 0.5Mcx_\alpha\ddot{\alpha} + k_y y = 0 \tag{2.3}$$

$$I_\alpha\ddot{\alpha} - 0.5Mcx_\alpha\ddot{y} + k_\alpha\alpha = 0 \tag{2.4}$$

Where M is the airfoil mass, I_α is the moment of inertia around the rotational axis and x_α is the distance between the elastic axis and center of gravity. If this is combined with equation 2.2, we get the modal mass and stiffness matrices as

$$\boldsymbol{M} = \begin{bmatrix} M_y & -0.5M_\alpha cx_\alpha \\ -0.5M_\alpha cx_\alpha & I_\alpha \end{bmatrix},\ \boldsymbol{K} = \begin{bmatrix} k_y & 0 \\ 0 & k_\alpha \end{bmatrix}$$

Clearly, the eigenmodes and frequencies play a large role in the dynamics of the system, thus changing them would have an impact on the flutter motion. The effects of changing the modal stiffness $\boldsymbol{K}$ is described by *Rayleigh's theorem*.

Rayleigh's Theorem

The previously mentioned critical velocity is often expressed as a reduced velocity

$$v_r = \frac{v_\infty}{\omega D} \tag{2.5}$$

where D is a characteristic length.[3] As one can see from this expression, increasing the frequency of the eigenmode in which flutter occurs could reduce the reduced velocity to a value below the critical point. One way in which this could be achieved is by increasing system stiffness, **Rayleigh's theorem on added stiffness** states that; "*for a system* $\{\boldsymbol{K}, \boldsymbol{M}\}$ *subjected to added stiffness* $\Delta\boldsymbol{K} > 0$ *its eigenvalues either stay or increase.*"[4]. Essentially this means that increasing the stiffness speeds up the dynamics of the system, and decreasing the stiffness slows them down. As implied by equation 2.5 this would hence reduce the reduced velocity, decreasing the risk of flutter.

3

Methods

A majority of the analysis in this project was carried out using commercial CFD-solver STAR-CCM+[6]. The results from these simulations were in part validated using various theoretical values and models. Within the program, the structural dynamics of the NACA0012 airfoil was modeled using a two-degree-of-freedom system.

3.1 Modeling of Dynamics

To minimize the amount of computational time needed for the analysis. The airfoil was approximated as a 2-dimensional 2 degree-of-freedom system with the rigid cross-section shape of the NACA0012 airfoil. The bending- and torsional stiffness of a 3-dimensional airfoil was modeled using a flexural and torsional spring as viewed in figure 3.1.

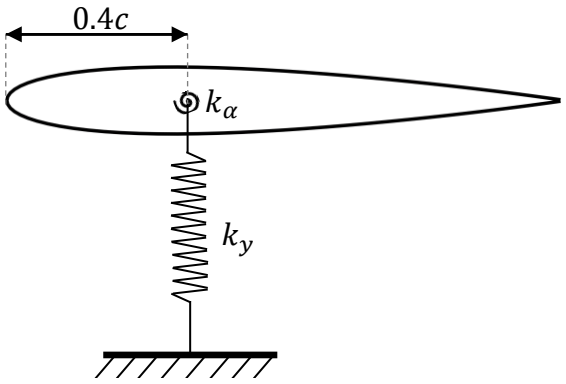

Figure 3.1: 2 degree-of-freedom model of the bending and torsional stiffness of the airfoil

As the center of gravity of the airfoil was found to be at approximately $0.4207c$, the positioning of the dynamic axis at $0.4c$ results in a non-zero x_α in equation 2.2.1. This means that there will be coupling between the rotational and translational degrees of freedom i.e. rotational motion will cause translational motion and vice versa.

This is of coarse a major simplification of the dynamics of the airfoil, However for the purpose of this project it is a useful simplification, in part because it removes the need to couple the CFD-solver with a structural solver but also because it limits the number of eigenmodes of the system.

3.2 STAR-CCM+

In the commercial software, a set of settings was chosen. Some of these were set based on theoretical knowledge, while some were set by empirical investigation of their effect on the resulting flow field and fluid structure interaction.

3.2.1 Physical Models

To properly catch the characteristics that could influence the aerodynamic flutter of an airfoil, unsteady RANS with compressible and viscous effects was used to model the fluid flow. All models used can be seen in table 3.1.

All y+ Wall treatment
Gas
Gravity
Ideal Gas
Implicit Unsteady
K-Omega Turbulence
Overset Conservation
Reynolds-Averaged Navier-Stokes
Segregated Flow
Segregated Fluid Temperature
Solution Interpolation
SST (Menter) K-Omega
Turbulent
Two Dimensional
Wall Distance

Table 3.1: Physical Models Used for STAR-CCM+ simulations

Although the mach number of the free stream flow is far below 0.3, which is a commonly used threshold for the need to account for compressibility, the *ideal gas* model was used instead of *constant density*. This makes it possible to capture the possible effects of sound wave generation on the airfoil behavior.

To model the turbulence, the $k - \omega$ SST model is suitable for its accurate modeling of near wall region[7]. This feature is valuable as the forces exerted on the solid by the fluid are of coarse of importance in the exitation of the dynamic system.

As seen in table 3.1, the equations were solved separately using the *segregated flow* model. This was chosen over the *coupled flow* model as there are no major compressible effects in the flow.

3.2.1.1 Initial Conditions

As initial conditions for the domain, the values changed from their standard settings are reported in 3.2.

Pressure	0.0 Pa
Static Temperature	294.15 K
Turbulence Intensity	0.05
Velocity	v_∞

Table 3.2: Initial Conditions used for STAR-CCM+ simulations

In addition to the set initial conditions the reference value for pressure was set to 101325 Pa.

3.2.2 Computational Domain & Meshing

As indicated in table 3.1, an overset approach was used to generate a suitable mesh for the spatial discretization. This allowed for cooperation between one overset mesh following the airfoil motion, resolving the boundary layer and downstream wake close to the trailing edge, and one background mesh to resolve the free stream and the turbulent wake further downstream. A schematic sketch of this setup can be seen in figure 3.2.

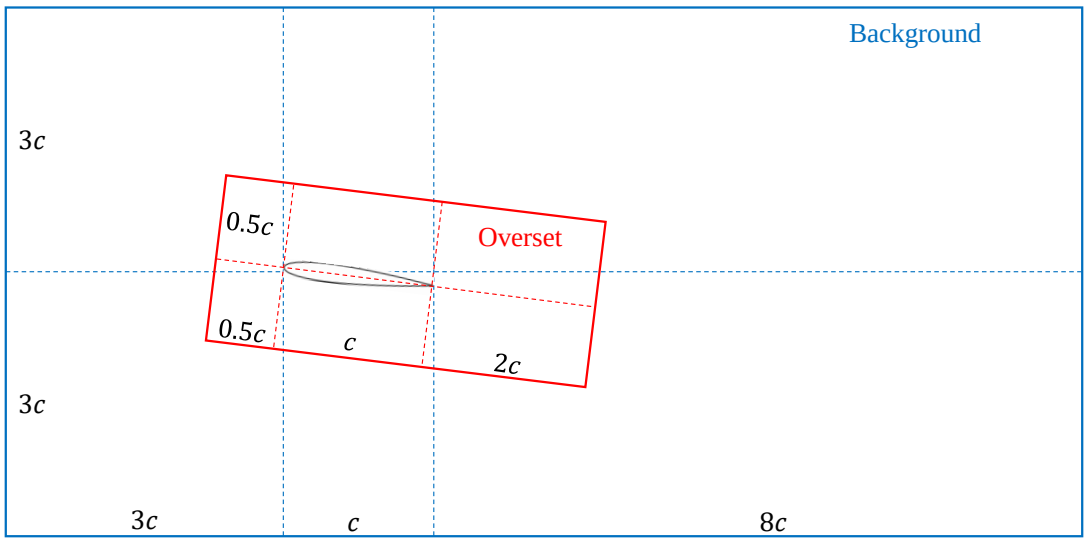

Figure 3.2: Computational domain. Split into a background region and a dynamic overset region. c denotes the coord length, defined in section 2.1.

For the overset mesh, the *quadrilateral mesher* was used together with the *prism layer mesher*. The prism layer mesher was used in order to resolve the boundary layer and properly catch the shear and pressure exerting forces on the airfoil. To resolve the turbulent wake developing within the overset region, a surface control with the *wake refinement* option was used. For the background mesh, only the quadrilateral mesher was used. In this region however, multiple volumetric refinements were used:

- **Overset interface refinement.** To ensure that the difference in cell size between the background and overset mesh was not too large, this refinement was set for the cells close to the overset region to have a size of similar order as the overset cells close to the background region.

- **Wake Refinement.** To make sure that the solver could catch the turbulent effects in the wake behind the trailing edge of the airfoil, a wake refinement was created in the background mesh. This spanned all the way from the overset mesh to the end of the domain. Towards the leftmost end of the wake refinement, a refinement similar to the overset interface refinement was created to ensure reasonable size difference between the background wake refinement and overset wake refeinement.

3.2.2.1 Mesh convergence study

Due to limitations on computational power and time, no mesh convergence study was carried out to ensure that the entire solution was independent of the meshing. The reasoning behind this was that with the limitations, the mesh size would not be feasible for time reasons. Rather than a traditional mesh independence study, efforts were made to ensure that the wall $y+$ along the airfoil surface was not too large. In accordance with the STAR-CCM+ documentation for *All Wall y+ Treatment*, the prism layer mesher was set up to make sure that the majority of the cells had a $y+$ value not in the buffer region of the boundary layer. This parameter was chosen to enable the best possible capture of the forces acting on the airfoil. In addition to this a steady state solver was run, and the obtained steady state lift coefficient was compared to theoretical values of equation 2.1. As this value was intended to be one of the main result parameters, it was considered important to make sure that it was evaluated decently.

3.2.2.2 Boundary Conditions

In the overset region, the boundary conditions applied were *Wall* for the airfoil surface, and *overset mesh* for the boundary between the overset and background region. In the background region, symmetry conditions were used for the upper and lower boundaries. For the inlet and outlet boundaries, the boundary conditions can be seen in table 3.3

Inlet	
Boundary type	Velocity Inlet
Static Temperature	294.5 K
Turbulence Intensity	0.05
Turbulent Viscosity Ratio	10
Velocity Magnitude	v_∞
Outlet	
Boundary type	Pressure Outlet
Static Temperature	294.5 K
Turbulence Intensity	0.05
Turbulent Viscosity Ratio	10
Pressure	0.0 Pa

Table 3.3: Boundary conditions for inlet and outlet boundaries of the background region of the computational domain

3.2.3 Solver Settings and Stopping Criteria

In the solvers used for the physical models described above, all settings except the time step of the *Implicit Unsteady* solver were left at their standard value. To properly resolve the airfoil dynamics and avoid divergence, the time step was set to 0.0002 seconds. For the solvers the stopping criteria presented in table 3.4 were used.

Continuity, Energy, X- and Y-momentum	
Criterion Option	Minimum
Logical Rule	And
Minimum Limit	1.0E-8
Maximum Inner Iterations	
Maximum Inner Iterations	15
Logical Rule	Or

Table 3.4: Stopping Criteria used to control STAR-CCM+ solvers

3.2.4 Dynamic Fluid Body Interaction

To simulate the dynamics of the rigid airfoil, STAR-CCM+'s DFBI-motion tool was used. This allowed motion to be free in the desired degrees of freedom, as well as definition of the constraints set to model the bending and torsion stiffness of the airfoil using *body couplings*. The settings for center of gravity and moment of inertia were chosen by numerical integration across the coordinates of the cross-sectional profile used to generate the geometry in STAR-CCM+, with material parameters for aluminium. For the airfoil 3-DOF 2D body, the following settings were set:

Free Motion	
X Motion	No
Y Motion	Yes
Z Rotation	Yes
Initial Values	
Angular Velocity	0
Center of Mass	[0.4207, 0.0, 0.0] m, m, m,
Moment of Inertia	12.4143 kgm^2
Velocity	[0.0, 0.0, 0.0]
Spring-Damper	
Position 1	[0.4, 0.0, 0.0] m,m,m
Position 2	[0.4cos($alpha_0), −0.4sin($alpha_0), 0.0] m,m,m
Relaxation Length	1 m
Coordinate System 1	Laboratory->Body 2D 1-CSys
Coordinate System 2	Laboratory
Elastic Coefficient	k_y
User Defined Coupling	
Position 1	[0.4, 0.0, 0.0] m,m,m
Position 2	[0.4cos($alpha_0), −0.4sin($alpha_0), 0.0] m,m,m
Relaxation Length	1 m
Coordinate System 1	Laboratory->Body 2D 1-CSys
Coordinate System 2	Laboratory
Moment Profile	[0.0, 0.0, k_α($Rotation + $alpha_0)]

Table 3.5: Settings used for the 3 DOF 2D DFBI body used to model the torsion and bending of the NACA0012 airfoil

3.3 Examining Flutter in Relation to Stiffness

As seen in section 2.2, a number of factors play a part in the vibrations of a structure, one of which is the stiffness. To examine the impact of stiffness changes (and hence changes in eigenfrequencies and reduced velocity in accordance with Rayleigh's theorem on added stiffness and equation 2.5) on flutter effects, the aforementioned mesh was used to run simulations at the given $v_\infty = 50$ m/s where both the bending and torsional stiffness were altered using a varying factor k_{fac}. Initially, one set of simulations was run to find a fairly small span of k_{fac} within which the stiffness of the critical flutter point should be located. After the limits of this span were determined, a second set of simulations were run in order to find the critical point and to examine the effect of stiffness changes on flutter effects.

To understand the effects of flutter on the performance of airfoil applications, the changes in lift coefficient over time for the cases close to the critical stiffness for flutter were also compared.

4

Results

4.1 Final Mesh

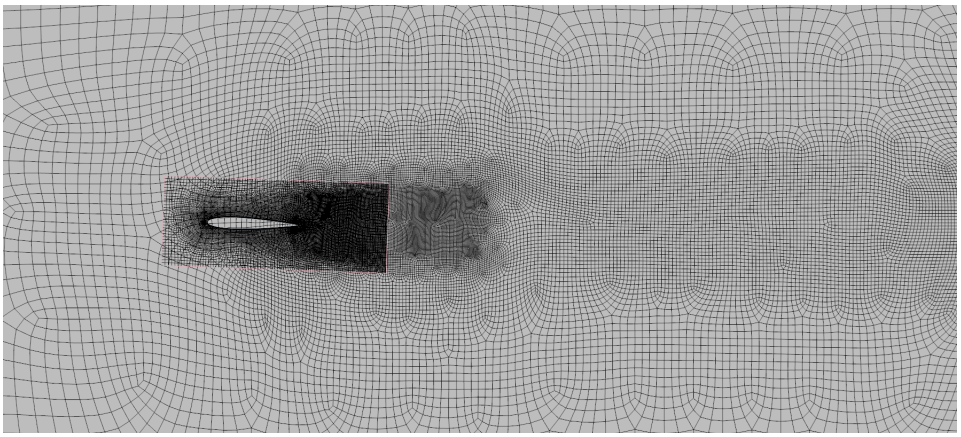

Figure 4.1: Final mesh used for simulations, with a cell count of 45294. By looking in the figure, one can distinctively see the interface between the overset and background mesh.

This section specifies the final mesh used for all of the simulation results presented in this chapter.

4.1.1 Mesh Quality

After creating a mesh according to the methods presented in section 3.2.2 with cell sizes that were considered good enough for the task at hand, a mesh of approximately 140 000 cells was obtained from STAR-CCM+'s automatic 2d mesher. However, as the dynamics of the rigid airfoil required a rather small time step to converge the solution, this mesh size required to much computational time for each simulation case. This lead to a significant increase in the mesh base size, which in turn lead to a clear decrease in performance regarding the parameters mentioned in section 3.2.2.1. To decrease the impact of the mesh coarseness on the results, a few specific improvements were made:

- The number of prism layers were increased in order to get a wall $y+$ below 5 for the majority of the airfoil surface.
- The cell size in the overset wake refinement was increased to better catch the effect of the near wake on the airfoil

- The interface refinement, both in general and in the wake refinement, was improved to better match the overset region

These refinements increased the number of cells in the coarse mesh from about 33 000 to about 45 000. As seen in figure 4.2, this led to a steady state C_L-value closer to the theoretical one, as well as a majority of the cell centers along the airfoil being in in the viscous sublayer rather than in the buffer layer.

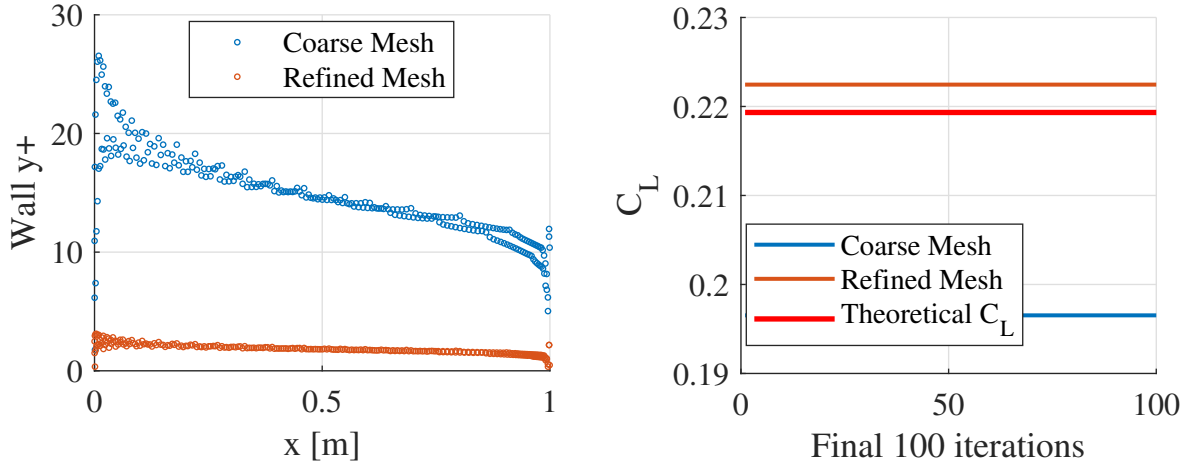

(a) $y+$ **(b)** C_L

Figure 4.2: Comparison of Wall $y+$ and C_L between the coarse mesh obtained after increasing cell size and the refined mesh obtained after minor refinements

4.1.2 Final Mesh Settings and Cell Count

The settings used after the mesh refinements were made can be seen in table 4.1 and 4.2 for the background mesh and overset mesh respectively.

Default Controls	
Base Size	0.5 m
Target Surface Size	120 % of base
Minimum Surface Size	1 % of base
Surface Growth Rate	Slow
Interface Refinement	
Custom Size	20 % of base
Wake Interface Refinement	
Custom Size	2.5 % of base
Wake Refinement	
Custom Size	7 % of base

Table 4.1: Background mesh settings

Default Controls	
Base Size	0.2 m
Target Surface Size	20 % of base
Minimum Surface Size	1 % of base
Surface Growth Rate	Slow
Number of Prism Layers	15
Prism Layer Stretching	1.5
Prism Layer Total thickness	0.025 m
Wake Refinement Refinement	
Size Type	Relative to base
Spread Angle	0.2 radian
Isotropic size	5 % of base
Wake Refinement Growth Rate	1..3

Table 4.2: Overset mesh settings

The mesh generated from these settings, as seen in figure 4.1 by the automatic 2d mesher had 45294 cells, of which 19936 were in the overset region and the remaining 25358 were in the background region.

4.2 Flutter

From the first simulations on the final mesh, it became clear that it was the eigenmode of the system dominated by rotational motion that would cause flutter issues at the given conditions. The difference between the motion in the 2 degrees-of-freedom can be seen in figure 4.3

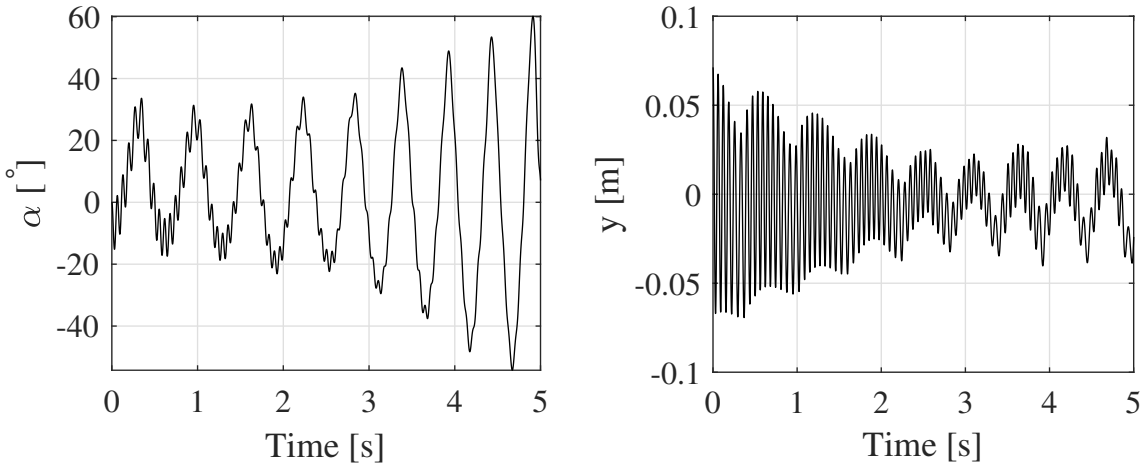

(a) Rotational motion **(b)** Translational motion

Figure 4.3: Time evolution of the airfoil motion at $k_{fac} = 1.2$. Within the initial five seconds, the rotation has started to diverge while the translation seems to be converging. The coupling of rotational and translational motion governed by equation 2.2.1 is particularly notable in **(b)**

Due to the dominance of the rotational motion at the given conditions. The comparison between models with varying stiffness will from here on out mainly focus on the differences in evolution of rotational amplitude.

4.2.1 Initial Simulations

From the initial set of simulations, the critical flutter boundary of the two-degree-of-freedom system of varying stiffness was found to be somewhere in the span $1.3 < k_{fac} < 1.35$.

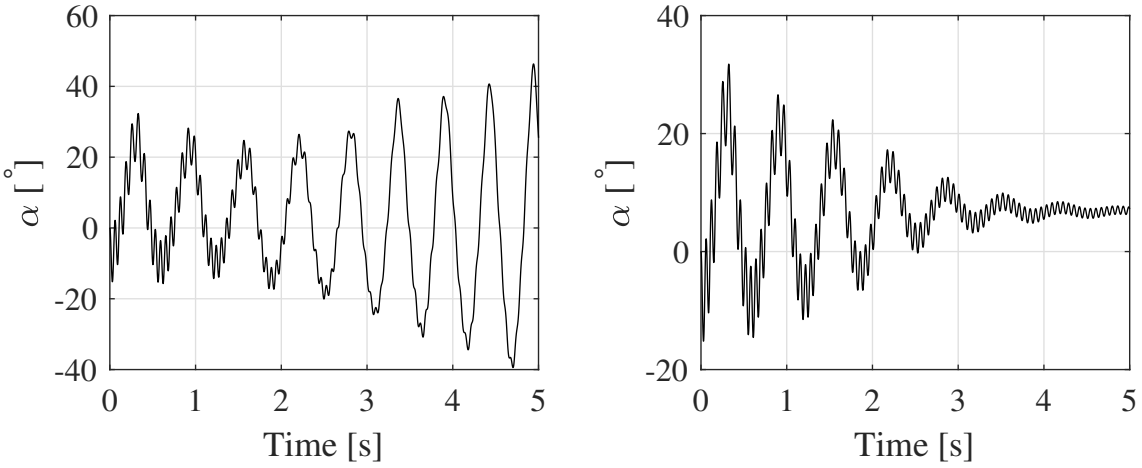

(a) $k_{fac} = 1.3$ **(b)** $k_{fac} = 1.35$

Figure 4.4: Time evolution of the airfoil rotation around the elastic axis. For the lower value of k_{fac} there is clear divergence of α, whereas for the higher value there is clear convergence to stable conditions.

From these results it was decided that the final simulations should be run in for stiffness values between $k_{fac} = 1.3$ and $k_{fac} = 1.35$.

4.2.2 Final Simulations

The torsional evolution in time for the simulations run in the span defined in the previous section can be seen in figure 4.5. The stiffness of the structure results in natural frequencies that give a reduced velocity around the critical value. Because of this, small changes causes the flutter to go from divergent to convergent.

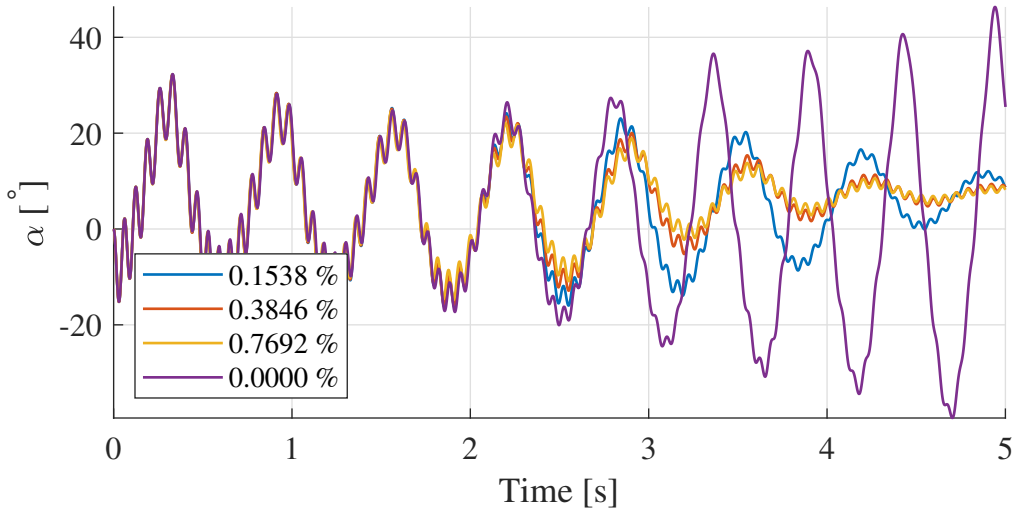

Figure 4.5: The results for simulations with $1.3 < k_{fac} < 1.35$. The legend values represent the relative stiffness increase from $k_{fac} = 1.3$. In this figure, it can clearly be seen how the increased stiffness decreases the reduced velocity from above to below the critical value.

It is interesting to note that initially, all stiffness values result in almost identical behavior. It is not until after a couple of seconds that we can start to see notable differences between the simulations. At this point the case with $k_{fac} = 1.3$ starts to diverge while the cases with increased stiffness start to converge. By looking at the difference between the converging cases we can also note that while in two of the simulations, the rotational oscillations converge at about the same rate, there is one case where the convergence rate is notably smaller. This is a sign that this stiffness is somewhere in the span between stable and unstable dynamics, close to the neutral behavior at the critical point.

4.2.2.1 Flutter impact on aerodynamic damping coefficients

The aerodynamic coefficients of the airfoil were of course, as indicated by equation 2.1, affected by the oscillating rotation. The effect of the flutter on the lift coefficient can be seen i figure 4.6.

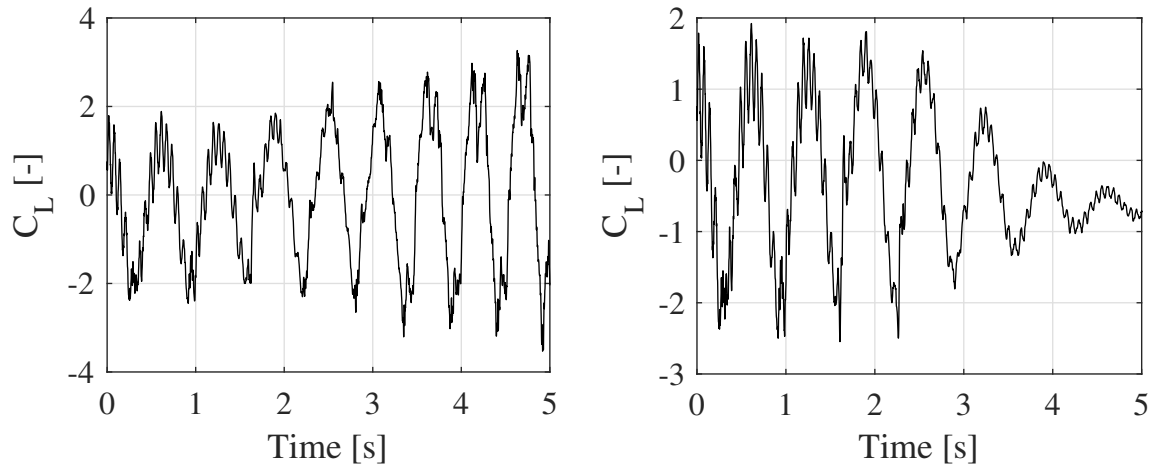

(a) $k_{fac} = 1.3$ **(b)** $k_{fac} = 1.305$

Figure 4.6: Time evolution of the lift coefficient of the NACA0012 airfoil. **a)** shows the dramatic impact of divergent flutter effects on the performance of airfoil components. As seen expected from figure 4.5, a stiffness increase of about 0.3 % has a large effect on the stability of the forces acting on the airfoil.

It is clear that the flutter can have negative effects on the performance of airfoil components. Given the central role of the generated lift in the purpose of the airfoil, flutter can as seen in figure 4.6 lead to unstable performance. In the case of changing flow conditions, it can also lead to unpredictable behavior when crossing the critical point of reduced velocity for flutter.

4.2.3 Simulation Quality

As discussed in section 3.2.2, the limitations of the project led to a meshing approach where only a few flow parameters were prioritized in order to achieve a sufficiently small mesh size. To examine the negative effects of this, the drag coefficient C_D and the turbulent viscosity ratio were examined for one of the simulations.

In addition to the lift coefficient, the ratio C_L/C_D was plotted for all simulations. As one can see in figure 4.7a the meshing approach resulted in some large instabilities in this

ratio. As the lift coefficient did not show this behavior, the spikes in the ratio must be a result of instabilities in C_D.

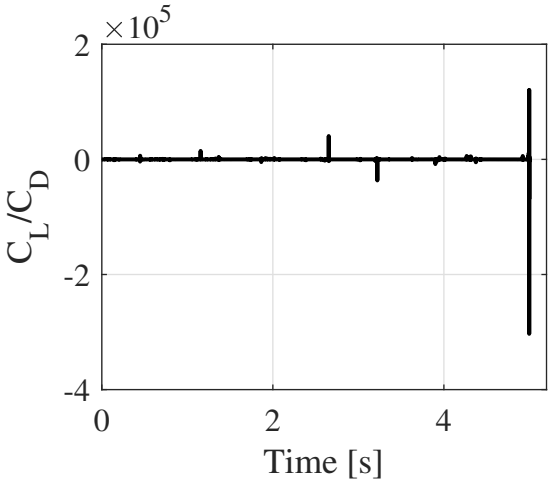

(a) C_L/C_D with $k_{fac} = 1.3$. Note use of scientific notation on y-axis

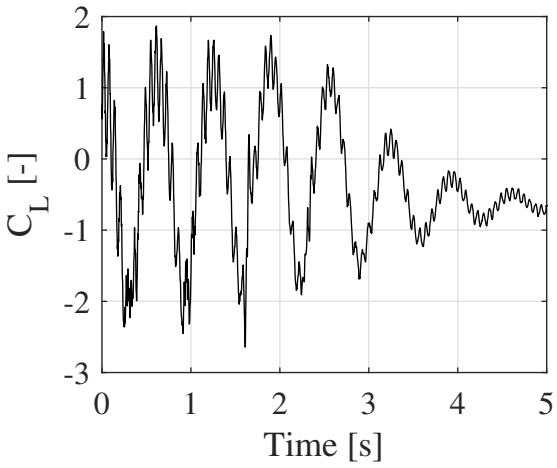

(b) C_L with $k_{fac} = 1.31$.

Figure 4.7: At some times steps, large instabilities can be seen in **a)**. Given the relative stability of C_L seen in **b**, the instabilities must stem from C_D.

The reason of this behavior is likely to be the insufficiently fine mesh. As the mesh refinements described in section 4.1.1 were decided on using a steady solver not allowing rotation of the airfoil, they did not take into account the effects of rotation on the turbulent wake. As seen in figure 4.8, the larger values of α resulted in parts of the turbulent wake moving outside of the introduced wake refinements.

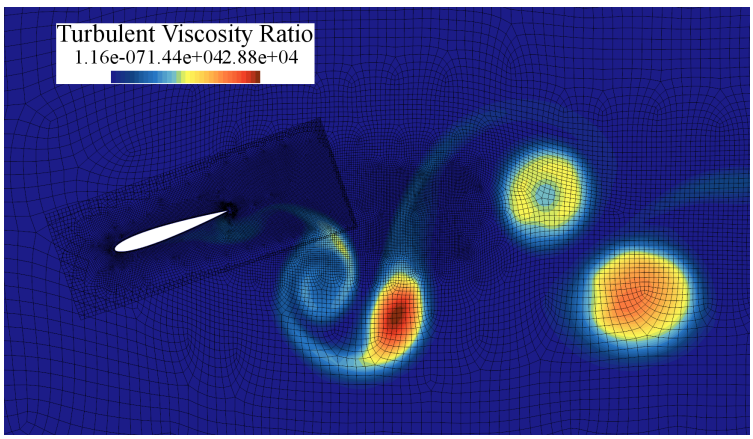

Figure 4.8: Turbulent Viscosity Ratio around the airfoil at a time step with large rotation. As senn around the trailing edge, large parts of the turbulent wake end up outside of the wake refinement

It is of course possible that that the low resolution of the wake could have resulted in unphysical effects on the airfoil and/or numerical issues as wake information propagated upstream towards the airfoil. In turn, this could be what lead to the unstable drag coefficient.

5

Conclusion

From the results it is clear that the structural stiffness is a parameter that can be experimented with as a countermeasure to flutter effects. This method of avoiding flutter could be particularly effective for structural components that are expected to operate at a specific set of conditions for a large part of their operating time. If in these cases, it becomes clear that a suggested design will be operating close to the critical point for flutter, thought through changes to the structural stiffness to increase the eigenfrequencies of modes of interest could ensure that that flutter is avoided. In a real world design decision it would however be wise to use a more accurate model of the system, for example a FEM model allowing for the inclusion of more than two eigenmodes. This would lead to the possibility of making sure that the avoidance of flutter in one eigenmode does not simply lead to an induction of flutter in another mode with a lower eigenfrequency.

Regarding simulation quality, it is clear that it is possible to catch flutter effects while using a fairly coarse mesh to reduce the computational cost. However guaranteeing accurate results would likely require a proper mesh convergence study ensuring mesh independence in the results. As clearly indicated in figure 4.7 the mesh used for this study does not ensure completely reliable results. If use of a smaller size mesh like the one used here is desirable, simulation results on a suggested mesh would have to be meticulously compared to experimental results to ensure that they provide realistic results for the parameters of interest.

References

[1] Mrinal Kaushik. "Thin Airfoil Theory". In: *Theoretical and Experimental Aerodynamics*. Singapore: Springer Singapore, 2019, pp. 127–144. DOI: 10.1007/978-981-13-1678-4_5. URL: https://doi.org/10.1007/978-981-13-1678-4_5.

[2] "Chapter 2 - Vibration Induced by Cross-Flow". In: *Flow-induced Vibrations (Second Edition)*. Ed. by Shigehiko Kaneko et al. Second Edition. Oxford: Academic Press, 2014, pp. 29–115. ISBN: 978-0-08-098347-9. DOI: https://doi.org/10.1016/B978-0-08-098347-9.00002-3. URL: https://www.sciencedirect.com/science/article/pii/B9780080983479000023.

[3] "Chapter 3 - Vibration Induced by External Axial Flow". In: *Flow-induced Vibrations (Second Edition)*. Ed. by Shigehiko Kaneko et al. Second Edition. Oxford: Academic Press, 2014, pp. 117–156. ISBN: 978-0-08-098347-9. DOI: https://doi.org/10.1016/B978-0-08-098347-9.00003-5. URL: https://www.sciencedirect.com/science/article/pii/B9780080983479000035.

[4] Thomas Abrahamsson. *Structural Dynamics and Linear Systems*. Chalmers University of Technology, 2019.

[5] Weixing Yuan, Rimple Sandhu, and Dominique Poirel. "Fully Coupled Aeroelastic Analyses of Wing Flutter towards Application to Complex Aircraft Configurations". In: *Journal of Aerospace Engineering* 34.2 (2021), p. 04020117. DOI: 10.1061/(ASCE)AS.1943-5525.0001232. eprint: https://ascelibrary.org/doi/pdf/10.1061/\%28ASCE\%29AS.1943-5525.0001232. URL: https://ascelibrary.org/doi/abs/10.1061/%5C%28ASCE%5C%29AS.1943-5525.0001232.

[6] Siemens. *STAR-CCM+*. Version 2021.3.1 (16.06.010-R8). Mar. 9, 2022. URL: https://www.plm.automation.siemens.com/global/pl/products/simcenter/STAR-CCM.html.

[7] H K Versteeg and W Malalasekera. *An Introduction to Computational Fluid Dynamics*. 2nd Edition. Pearson, 2007.

MASTER PROGRAM APPLIED MECHANICS
CHALMERS UNIVERSITY OF TECHNOLOGY
Gothenburg, Sweden
www.chalmers.se

CHALMERS
UNIVERSITY OF TECHNOLOGY